A Solid-State NMR Study of Structure and Segmental Dynamics of Semicrystalline Elastomer-Toughened Nanocomposites

Jiri Brus,* Martina Urbanová, Ivan Kelnar, and Jiří Kotek

Institute of Macromolecular Chemistry, Academy of Sciences of the Czech Republic, Heyrovsky Square 2, 162 06 Prague 6, Czech Republic

Received March 6, 2006; Revised Manuscript Received June 5, 2006

ABSTRACT: Significant enhancement in toughness and elongation at a break in nanocomposites based on polyamide-6 (PA6) and silicate platelets (MMT, 5 wt %) was achieved by co-adding of a small amount of ethylene−methyl acrylate copolymer (EMA, 5 wt %). To investigate the observed changes in this triple component system at a molecular level, motional behavior of polymer segments was probed by recently developed 2D techniques of $^1H-^{13}C$ dipolar solid-state NMR spectroscopy. Owing to measurements performed separately in amorphous and crystalline domains, a large collection of high-quality site-specific dipolar profiles could be analyzed with respect to a distribution of motional amplitudes: (i) in both crystal modifications as well as in "constrained" domains of the amorphous phase of PA6, the amplitudes of rotational-diffusion motion of CH_2 groups (10−33°) increase from NH and CO groups toward the central part of the repeat units, (ii) comparing both crystal modifications, less-tight packing of polymer chains in γ-form increases fluctuation angle about 5°, and (iii) the presence of silicate platelets in amorphous PA6 matrix enhances motional amplitudes of polymer segments in nanocomposites. The determined order parameters were further used to estimate an upper bound for the change in the Gibbs free energy resulting from structural restrictions occurring in the investigated systems. As a result of the increased conformational entropy, the Gibbs free energy in nanocomposites is somewhat reduced (ΔG = 0.4−0.5 kcal/mol). This fact, together with temperature-induced enhancements of the motional amplitudes, supports the explanation that fast and relatively low-amplitude motions occurring in the glassy state of polyamide-6 can be considered as mechanically active, and as a potential supplementary factor that may help to enable the larger-amplitude motions (jumps) associated with glass-transition temperature. Finally, the enhancement of ductility observed in the triple-component system was attributed to the formation of EMA copolymer domains that are surrounded by clay platelets. The size of these "core−shell" particles is sufficiently large (50−200 nm) for the internal dynamics of polymer chains not to be significantly hindered by rigid components. Polymer chains in these completely phase-separated domains exhibit large-amplitude motions and undergo the most prominent temperature-induced changes.

Introduction

New types of polymer systems containing nanometer-size particles offer exciting prospects for material science.[1] The great potential of these materials follows from the fact that uniform dispersion of nanosized particles leads to an ultralarge interfacial area. Consequently, these materials have recently received significant attention because of improvement in mechanical and thermal properties, which result from synergistic effects between polymers and suitably chosen nanoparticles.[2]

In these complex materials, however, one cannot expect simple relations between material properties and the composition of polymer systems. A large interfacial area and significantly enhanced surface-to-volume ratio causes unexpected changes in molecular dynamics. Confined polymer chains spatially close to the nanofiller are immobilized, which causes T_g to shift to a higher temperature. At the same time, it is supposed that the enhanced chain mobility existing at the surface causes a reduction of T_g in thin polymer films, porous materials, and composites with poor interfacial adhesion.[3,4] Since these effects oppose each other, it is no surprise that both decrease[5−8] and increase[9−11] of glass-transition temperature (T_g) in nanocomposites has been reported. In polymer systems based on polyamide-6 (PA6) and layered silicates (montmorillonite, MMT) T_g mostly decreases in "dry" samples,[12,13] while in the presence of adsorbed moisture, rather minor elevation of T_g was observed.[13] The understanding of these phenomena is further complicated by the formation of the thermodynamically unstable crystal γ modification.[14] That is why the disclosure of the fine relations between all acting contributions and final properties of polymer nanocomposites requires deep investigation of the structure and dynamics of polymer chains. For such a task, we need additional techniques complementary to traditional tools such as WAXS and TEM.

It has been shown several times that solid-state NMR spectroscopy is an excellent method providing information about the structure and dynamics of nanocomposites without requiring long-range order.[15−23] Among all NMR techniques, relaxation measurements play a dominant role in this regard, as they offer site-specific information about time scales of the motional processes. However, spin relaxation does not depend only on the rate of local fluctuation but also on the concentration of paramagnetic centers such as Fe^{3+} ions. That is why it is not surprising that the interpretation of relaxation data for nanocomposites based on clay minerals is complicated. It is well-known that naturally occurring aluminosilicates contain small amounts of Fe^{3+} ions substituting Al^{3+} in octahedral sites. Due to this fact, the spin relaxation of protons localized near to the silicate surface is accelerated. Subsequent fast $^1H-^1H$ spin diffusion propagates this effect to more distant regions of polymer matrix. Consequently, the measurement of T_1 (^1H)

* To whom correspondence should be addressed. E-mail: brus@imc.cas.cz. Telephone: +420 296 809 380. Fax: +420 296 809 410.

10.1021/ma0604946 CCC: $33.50
Published on Web 07/12/2006

relaxation times is better suited for the determination of the relative exfoliation degree, as has been nicely demonstrated by Van der Hart et al.[24] This phenomenon (without spin-diffusion propagation) can be expected also when measuring relaxation of ^{13}C magnetization.

An alternative approach how to obtain information about molecular dynamics usually employs the line-shape analysis of deuterium NMR spectra.[25] The requirement of labeled materials, however, renders application of this technique impractical for a solution of some academic and industrial problems where synthetic effort necessary to selectively label the molecules can be nearly daunting. Recent advances in NMR spectroscopy improved sensitivity and resolution in such a way that a basic experimental concept intended for labeled materials can be partially used also for systems at natural isotopic abundance. This possibility can be realized by site-specific measurement of one-bond $^1H-^{13}C$ dipolar couplings (D_{CH}) in CH or CH_2 groups forming the polymer backbone. Assuming constant length of the C−H chemical bond, any reduction of the dipolar interaction compared with the theoretical rigid limit value ($D_{CH,rig}$ = 22.7 kHz, r_{CH} = 1.09 Å) can be attributed to the released internal motion.

Up to now, various techniques have been developed. Among others, analysis of a sideband pattern produced by rotor-encoded experiments such as recoupled polarization transfer via heteronuclear dipolar order rotor encoding (REPT-HDOR) or rotor-encoded REDOR (REREDOR) allow for a precise determination of dipolar coupling constants.[26,27] However, necessity of ultrafast magic angle spinning (MAS, ca. 25 kHz) requires utilization of small-diameter rotors in which the amount of the sample is very small, ca. 8−10 mg. This reduces sensitivity of NMR experiments especially for disordered solids. An alternative approach is offered by the techniques based on Lee−Goldburg[28] cross polarization (LG-CP)[29,30] such as phase-inverted LG recoupling under MAS (PILGRIM)[31] and/or the sideband version[32] of polarization inversion spin exchange at magic angle (PISEMA) technique,[33] which provide high-quality measurement of D_{CH} in powdered solids at moderate MAS (10−15 kHz). Unfortunately, polymer nanocomposites are very often semicrystalline and motionally heterogeneous systems producing complex NMR spectra with a poor resolution of ^{13}C NMR signals of various modifications. An analysis of motional amplitudes in semicrystalline polymers then requires application of techniques providing separate measurements of D_{CH} in various domains according to their internal dynamics.[34]

In this contribution, we demonstrate the experimental procedures providing high-quality data about polymer chain dynamics in complex nanocomposites. We focused our attention on the precise measurements of motional amplitudes of polymer segments in various polymer/crystal forms of one of the most popular groups of nanocomposites based on polyamide-6 matrix and silicate platelets. At this opportunity, we investigated the influence of clay nanoparticles on the dynamics of polymer segments in amorphous phase. We present here a large collection of site-specific dipolar profiles, which were analyzed and discussed with respect to the distribution of possible motional modes of polymer segments. Consequently the geometry of motion for almost every polymer segment was described without the necessity of isotopic enrichment. The obtained experimental data are finally discussed in an attempt to explain changes in T_g and other mechanical properties observed in the investigated nanocomposites.

We believe that the concepts behind these experiments are of interest for all chemists who work with complex polymer systems and use solid-state NMR for characterization of segmental dynamics and design of new polymer products.

Table 1. Composition and Mechanical Behavior of the Prepared Materials (σ_M, Tensile Strength, ϵ_b, Strain at Break, E, Young's Modulus, and a_t, Tensile Impact Strength)

sample	composition	σ_M (MPa)	E (MPa)	a_t (kJ·m^{-2})	ϵ_b (%)
PA6	PA6 (Ultramid B5)	73.7	1620	16.5	160
NC	PA6/C30B = 95/5	94	2600	18	90
NC/EMA	PA6/C30B/EMA = 90/5/5	82	2540	42	140

Experimental Methods

Materials. All products listed below were used as purchased: cloisite 30B (Southern Clay Products, Inc., USA) montmorillonite modified with alkylbis(2-hydroxyethyl) methylammonium chloride, alkyl is derived from tallow (silicate content 74 wt %), Polyamide 6 (PA6) Ultramid B5 (BASF, Germany) M_n = 42 000, and ethylene-methyl acrylate (70−30%) copolymer (EMA) Lotryl 28MA07.

Nanocomposite Preparation. Prior to mixing, PA6 and clay were dried at 85 °C and 70 °C, respectively, for 12 h in a vacuum oven. The blends were prepared by mixing the components (PA6, Cloisite 30B, and in some cases, EMA) in a Brabender Plasti-Corder W50ETH mixer at 255 °C and 45 rpm for 10 min. The material removed from the chamber was immediately compression molded at 250 °C to form 1-mm-thick plates. Strips cut from these plates were used for preparation of dog-bone specimens (type 1BA according to ISO527 standard) in a laboratory microinjection molding machine (DSM). The barrel temperature was 265 °C, that of the mold, 80 °C. All the tested samples have the same thermal history. The reported values of clay content in wt % of Cloisite C30B are not corrected for pure silicate content. Composition of tested polymer systems is summarized in Table 1.

Testing. Tensile tests were carried out at 22 °C using an Instron 5800 apparatus at a crosshead speed of 20 mm/min. The tensile strength σ_M, strain at break ϵ_b, and Young's modulus E were evaluated. Reported values are averages of 10 individual measurements. Corresponding variation coefficients do not exceed 5%. Tensile impact strength, a_t, was measured with one-sided notched specimens using a Zwick hammer with an energy of 4 J (variation coefficient 10−15%). Dynamic mechanical thermal analysis (DMTA) was done in single-cantilever mode using DMA DX04T apparatus. Results of the above-mentioned testing procedures are listed in Table 1.

NMR Spectroscopy. All NMR spectra were measured using Bruker Avance 500 WB/US NMR spectrometer (Karlsruhe, Germany, 2003) at a magic angle spinning (MAS) frequency of 12 kHz. In all cases, the dried samples were placed into the ZrO_2 rotors and stored under silica gel to prevent rehydration. Site-specific measurements of one-bond $^1H-^{13}C$ dipolar couplings in semicrystalline polymers systems were performed by our recently developed amplitude-modulated PISEMA experiments.[34] Although the detailed analysis of these two recoupling techniques and setup of experimental parameters have been introduced in our previous contribution,[34] we present here a short description for clarity (see also Supporting Information): in both cases one-bond heteronuclear $^1H-^{13}C$ dipolar couplings are indirectly detected during the amplitude-modulated PISEMA recoupling sequence[32] (t_1). Torchia's approach using 4−10 s delay (τ_2) between flip-back and read-out pulses[35] was applied for the separate measurements of $^1H-^{13}C$ dipolar couplings in crystallites (Scheme 1a, T_1-filtered AM-PISEMA). Careful optimization of the experimental parameters (e.g., long T_1 filter) ensures the high-quality separation of crystalline and amorphous contributions and minimizes contamination of the selective NMR spectra by unwanted magnetization. Separate measurements of $^1H-^{13}C$ dipolar interactions in the amorphous phase require efficient suppression of ^{13}C magnetization originating from the crystallites. This is achieved by a train of 90° pulses, which is followed by a short delay (τ_1). The train of pulses effectively saturates transitions of ^{13}C spins in both crystalline and amorphous

Scheme 1. Schematic Representation of the Applied Pulse Sequences

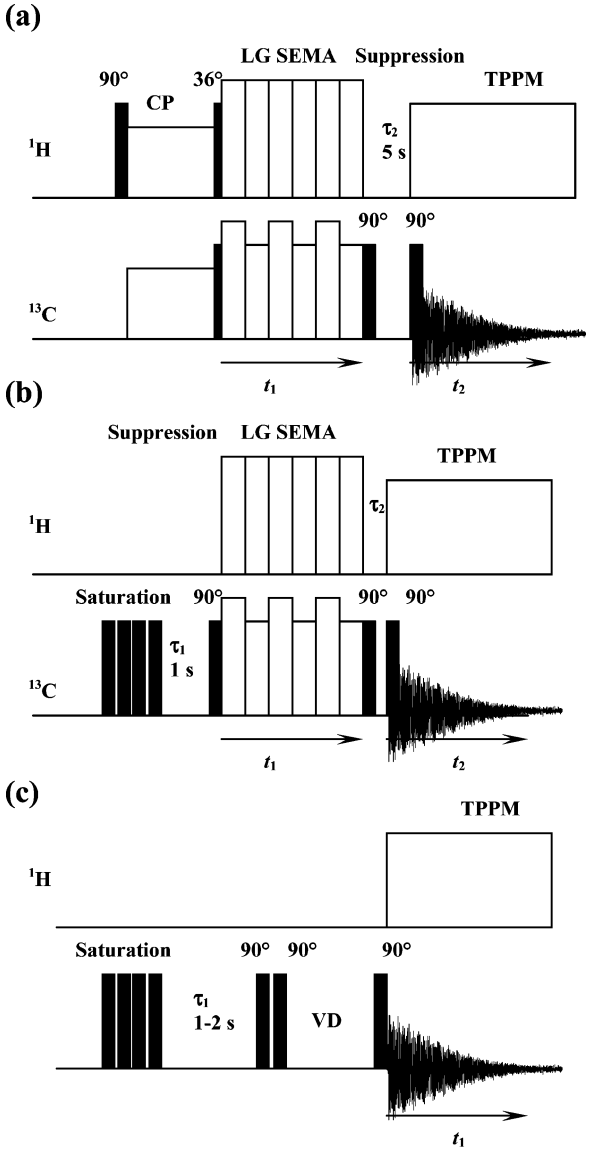

(a) 2D T_1-filtered AM-PISEMA experiment[34] modified by flip-back and read-out pulses to detect D_{CH} of the crystalline phase only; (b) 2D direct-polarization AM-PISEMA experiment modified by a train of saturation pulses to detect the D_{CH} of the amorphous phase only;[34] (c) $T_1(^{13}C)$ relaxation experiment modified to detect magnetization of the amorphous phase only.

phases, while the short delay (τ_1) 1−2 s brings ^{13}C magnetization of the amorphous phase back to the *z* direction. A subsequent 90°-(^{13}C) pulse excites magnetization of the amorphous phase only. During the following amplitude-modulated recoupling sequence, the $^1H-^{13}C$ dipolar oscillations originating from the amorphous phase are observed (Scheme 1b, direct-polarization AM-PISEMA).

A similar approach was used to measure T_1 (^{13}C) relaxation selectively in the amorphous phase. After the train of 90° pulses followed by the short delay (τ_1), a pair of flip-back and read-out pulses was inserted. The variable delay (VD) between them ranges from 0.1 to 2 s (Scheme 1c). Standard Torchia's T_1 (^{13}C) relaxation experiments[35] with variable delay (4−60 s) were performed to probe the internal motions at nanosecond time-scales selectively in crystallites. The degree of exfoliation of silicate platelets in a polymer matrix was probed by the inversion recovery T_1 (^1H) relaxation experiment. The intensity of the B_1 (^1H) field of TPPM (two-pulse phase-modulated) decoupling[36] corresponds to $\omega_1/2\pi = 89.3$ kHz. Taking into account frictional heating of the samples during fast rotation,[37] all NMR experiments were performed at 308

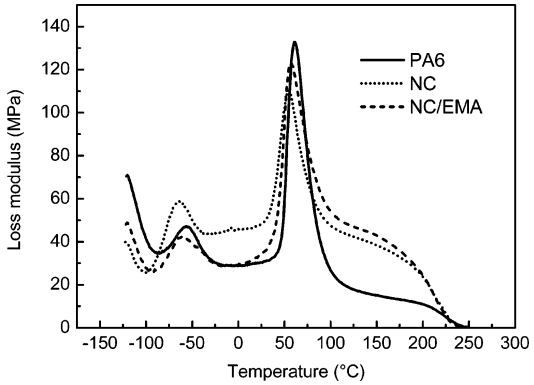

Figure 1. Temperature dependence of loss modulus of PA6 and its nanocomposites.

Scheme 2. Structure and Numbering of Carbons in Repeat Unit of PA6

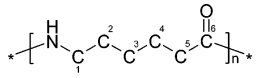

and in some cases at 318 K (precise temperature calibration was performed).

Results

Mechanical and Thermomechanical Properties. Before the analysis of internal dynamics, structure and basic mechanical properties of neat polyamide-6 and its nanocomposites were described (Table 1). As follows from temperature dependences of loss modulus, the presence of the clay sheets leads to a slight depression of the T_g peak and the formation of a high-temperature shoulder. At the same time, the glass transition of the nanocomposites is shifted to a low temperature (ca. 55 °C, Figure 1). The significantly enhanced Young's modulus of the nanocomposites in comparison with the neat PA6 is the first indirect evidence of a high extent of clay exfoliation.

Composition of Polymer Matrix. Although the obtained ^{13}C CP/MAS NMR spectra are relatively complex with overlapping signals of all polymorphs, large differences in ^{13}C NMR chemical shifts of C1 carbons (Scheme 2) provide characteristic markers distinguishing both crystal forms (α and γ). In addition, differences in segmental dynamics permit recording of ^{13}C NMR spectra separately for the mobile amorphous phase and the rigid crystallites (Figure 2). Following the literature data,[38] signals of both crystal modifications and amorphous phase were easily

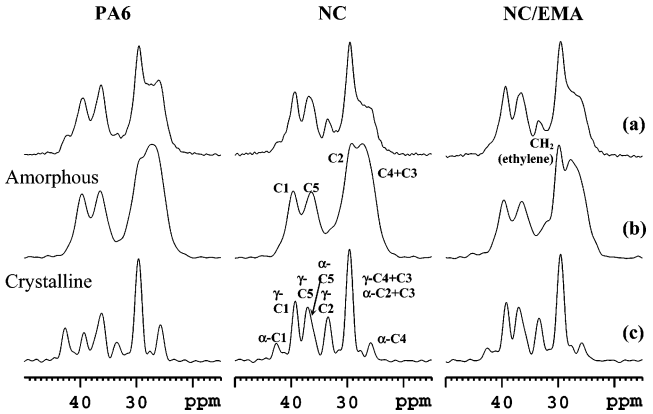

Figure 2. Standard ^{13}C CP/MAS NMR spectra of pure polyamide PA6 and its nanocomposites (NC and NC/EMA) reflecting both amorphous and crystalline phases (a), selective ^{13}C MAS NMR spectra reflecting the amorphous phase only (b), and selective T_1-filtered ^{13}C CP/MAS NMR spectra of crystallites (c).

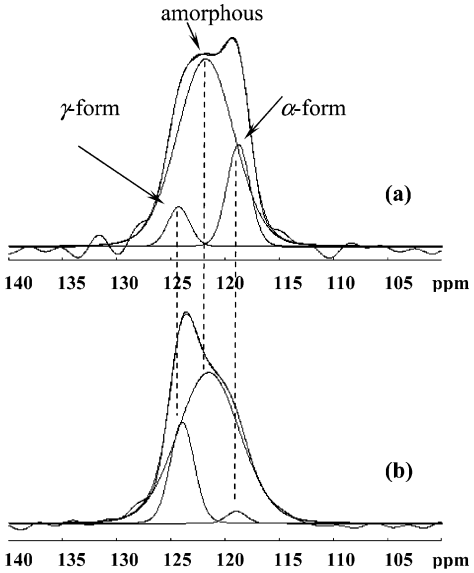

Figure 3. Decomposition of ^{15}N CP/MAS NMR spectra of pure PA6 (a) and its nanocomposite NC (b).

assigned. Subsequent decompositions of ^{13}C CP/MAS and ^{15}N CP/NMR spectra (Figure 3) confirm that the amorphous phase is the dominant component (ca. 70 ± 2%) and the degree of overall crystallinity does not depend on the presence of silicate particles or EMA copolymer.

As expected the α-form is the main crystal modification in pure PA6, while the presence of silicate sheets promotes the development of γ-form and leads to a corresponding decrease in α-phase content. Consequently, the significant decrease in the α/γ ratio (Table 2) is another evidence of a good dispersion of silicate platelets. The high degree of exfoliation follows also from the measurement of ^{1}H longitudinal relaxation times. As reported previously,[24,39] an intimate mixing of polymer chains and silicate platelets produces significant shortening of relaxation times in nanocomposites (Table 2). Finally, a relatively high degree of exfoliation of silicate platelets in the investigated nanocomposites was previously confirmed by TEM and WAXS measurements.[40,41] From the presented TEM micrograph of the triple-component nanocomposite NC/EMA (Figure 4), it is clear that EMA copolymer is phase-separated and forms relatively large domains. While silicate platelets are well dispersed in a PA6 matrix, they are quite absent in EMA domains and rather produce a clay shell around these particles. Consequently, on the resulting interface, intercalated aggregates of silicate minerals can be expected. The phase separation of the EMA elastomer within the whole volume of the sample was confirmed by static ^{1}H NMR spectra and ^{1}H−^{1}H spin diffusion experiments, providing also additional evidence that the average size of EMA domains is ca. 50−200 nm (Supporting Information).

Dynamics of Polymer Segments. Bearing in mind all the above-mentioned limitations of relaxation experiments, we performed some measurements in order to roughly probe changes in the time scales of internal motions of polymer chains separately in the amorphous phase and in both crystal forms.

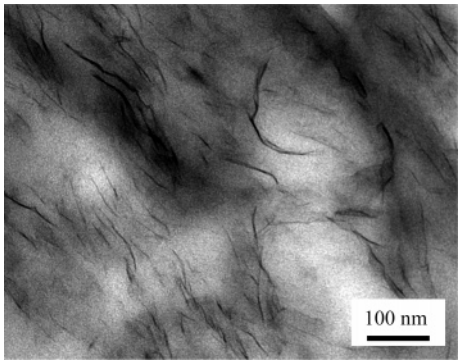

Figure 4. TEM micrograph of PA6/C30B/EMA 95/5/5 nanocomposite. Light areas represent the EMA-rich phase partially surrounded by clay platelets.

Table 3. T_1 (^{13}C) Relaxation Times of Methylene Units (C1−C5) in Amorphous Phase and C1 Groups in Crystal Modifications α and γ

	T_1 (^{13}C), s					
			amorphous			
sample	α-form C1	γ-form C1	C1	C5	C2	C3 + C4
PA6	38	26	1.11	0.97	0.84	0.64
NC	37	23	0.95	0.92	0.79	0.60
NC/EMA	33	20	0.88	0.90	0.69	0.58

Although fluctuations at nanosecond time scale rarely occur in crystallites, as reflected by long T_1 (^{13}C) relaxation times, the observed differences (Table 3) indicate slightly enhanced dynamics of CH_2 in γ modification. On the other hand, high-frequency motions including wobbling of all methylene groups, dominates over reorientation of polymer segments in the amorphous phase because corresponding T_1 (^{13}C) relaxation times are very short (0.6−1.1 s, Table 3). Slight shortening of relaxation times in amorphous domains detected in the nanocomposites can indicate enhanced segmental dynamics. However, the observed differences are so small that they can be attributed to the presence of Fe^{3+} ions.

Motion-Averaged Dipolar Couplings and Order Parameters. Because of the limited ability of the relaxation experiments, we focused on the characterization of polymer chain dynamics through the site-specific measurement of ^{1}H−^{13}C dipolar spectra providing an order parameter (S) that contains information about motional amplitude for every structure unit. For organic solids, the recently developed amplitude-modulated 2D PISEMA experiments[34] provide dipolar spectra (Figure 5) in which the splitting ($\Delta\nu$) reflects the dipolar coupling constant according to a simple relation: $\Delta\nu = D_{CH}/(\sqrt{2})\sin\theta_m$, where θ_m is 54.7°. Motionally induced averaging of D_{CH} then can be expressed by an order parameter, S, which is the scaling factor between the measured coupling strength (D_{CH}) and rigid-limit value ($D_{CH,rig}$).[42] Theoretically, for a typical rigid segment C−H, the dipolar splitting observed in the spectrum is ca. 13.1 kHz. In practice, however, owing to vibrational averaging of the C−H bond at room temperature and experimental imperfections, the rigid-limit value of the dipolar splitting is smaller, found to be 12.0 kHz based on model compounds measurements (crystalline alanine and glycine, Figure 5).

Table 2. Morphology of the Investigated Polymer Systems Obtained by Analysis of ^{15}N and ^{13}C CP/MAS NMR Spectra and T_1 (^{1}H) Relaxation Times of Methylene Units

			^{15}N CP/MAS NMR			^{13}C CP/MAS NMR		
sample	α/γ	T_1^{1H} (s)	α-form (%)	amorph (%)	γ-form (%)	α-form (%)	amorph (%)	γ-form (%)
PA6	4.70	1.60	23	72	5	24	71	5
NC	0.22	0.63	6	69	25	5	69	26
NC/EMA	0.23	0.62	5	72	23	5	73	22

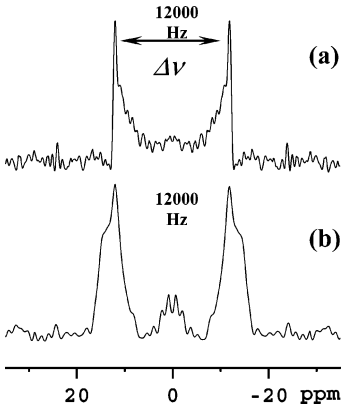

Figure 5. $^{13}C-\{^1H\}$ dipolar spectra of the CH group of alanine (a) and the CH_2 unit of glycine (b). The splitting of the dipolar spectra ($\Delta\nu$) reflects the dipolar coupling constant (D_{rig}).

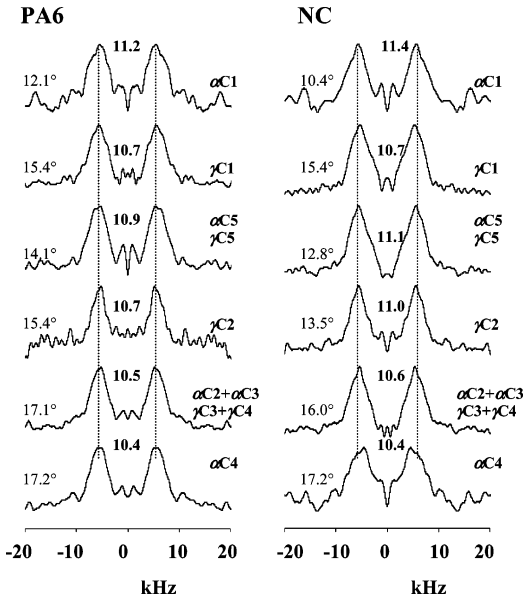

Figure 6. $^{13}C-\{^1H\}$ dipolar spectra of CH_2 units in crystallites of polyamide chains in neat PA6 and its nanocomposite (NC). The splitting in kHz ($\Delta\nu$) reflecting motionally averaged dipolar couplings (D_{CH}) is shown between the maxima, and the corresponding rms amplitude is at the left side of each spectrum.

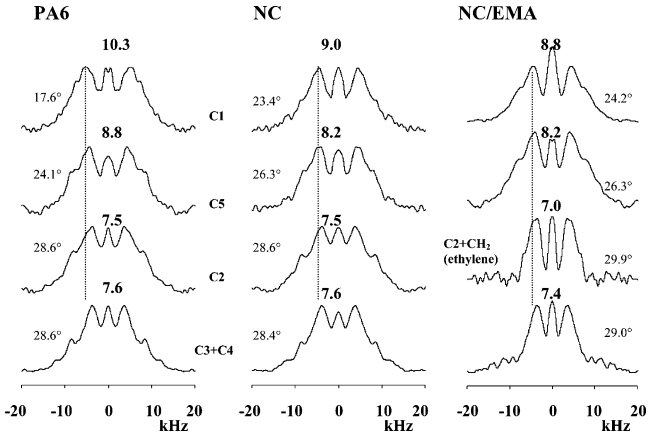

Figure 7. $^{13}C-\{^1H\}$ dipolar spectra of CH_2 units in the amorphous phase of polyamide chains in neat polyamide (PA6) and its nanocomposites (NC and NC/EMA) measured at 308 K. The splitting in kHz ($\Delta\nu$) reflecting the motionally averaged dipolar coupling constant (D_{CH}) is shown between the maxima, and calculated rms amplitude is at the left side of each spectrum. Experimental error ca. ±0.7° was estimated from two repeated experiments.

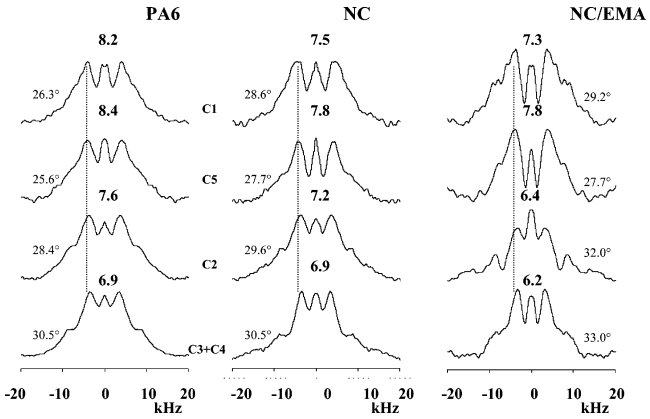

Figure 8. $^{13}C-\{^1H\}$ dipolar spectra of CH_2 units in the amorphous phase of polyamide chains in neat polyamide (PA6) and its nanocomposites (NC and NC/EMA) measured at 318 K. The splitting in kHz ($\Delta\nu$) reflecting the motionally averaged dipolar coupling constant (D_{CH}) is shown between the maxima and calculated rms amplitude is at the left side of each spectrum. Experimental error ca. ±0.7° was estimated from two repeated experiments.

For polymer segments in the crystalline phase, the T_1-filtered AM-PISEMA experiment (pulse sequence 1a) provided dipolar profiles (Figure 6) from which the order parameters ranging from 0.95 to 0.86 were determined. The line shapes of these dipolar spectra are comparable with the dipolar profile of a glycine CH_2 unit. Hence, almost uniform order parameter for each type of methylene over the whole crystallite can be expected. On the other hand, the order parameter of the methylene group is not uniform within the repeat unit and decreases from NH and CO groups to the central part (C3 and C4, Figure 6). Direct comparison of the dipolar profiles produced by C1 methylene groups in both crystal modifications further revealed that the notably reduced dipolar coupling constant is in γ-form (ca. 0.5−0.7 kHz).

The second technique selectively exciting magnetization originating from mobile components (direct polarization AM-PISEMA, sequence 1b) was then utilized to record the site-specific dipolar profiles in amorphous phase. In contrast to the previous case, the pattern of the dipolar spectra (Figure 7) is significantly different and the three main features are fairly discernible. At first, the dipolar spectra (the doublets) are less resolved. Second, the splitting between the maxima is reduced. And third, zero-frequency signals are clearly apparent.

The first phenomenon results from a superposition of several dipolar doublets. It means that, in the amorphous phase, motional amplitudes of polymer segments are not uniform over the whole sample and exhibit larger variation contrary to almost uniform dynamics of polymer segments in crystallites. That is why these dipolar spectra had to be decomposed by a computer peak fitting, and the dipolar splitting was determined from the best fit as discussed later. Similarly, as in the crystallites, the order parameter, S, decreases toward the central part of repeat units (from $S = 0.86$ to 0.62). Further, it was found out that the motionally averaged dipolar couplings in nanocomposites are notably smaller than that in neat PA6 (Figure 7).

This difference is clearly discernible in the dipolar spectra of C1 and C5 groups. As the observed differences surely exceed the estimated experimental error, this finding indicates enhanced dynamics of polymer chains in nanocomposites. Finally, it must be mentioned that the dipolar spectra separated for C2 methylene units in NC/EMA nanocomposite exhibit slightly different shapes (Figures7 and 8). With high probability, this follows from the interference and spectral overlap with signals of ethylene

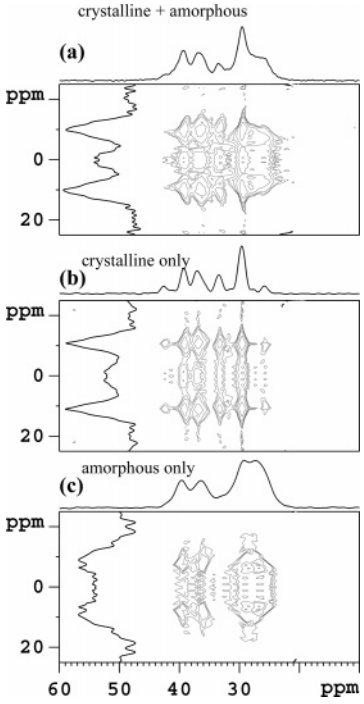

Figure 9. Two-dimensional spectra separating the ^{13}C isotropic chemical shift vs $^{13}C-\{^1H\}$ dipolar profiles obtained for nanocomposite NC: nonselective measurement detecting both the amorphous and crystalline phase (a), selective experiments recording dipolar profiles for the crystalline phase (b), and for the amorphous phase only (c). Slices at ca. 39 ppm reflecting $^{13}C-\{^1H\}$ dipolar profiles are shown within the 2D spectra.

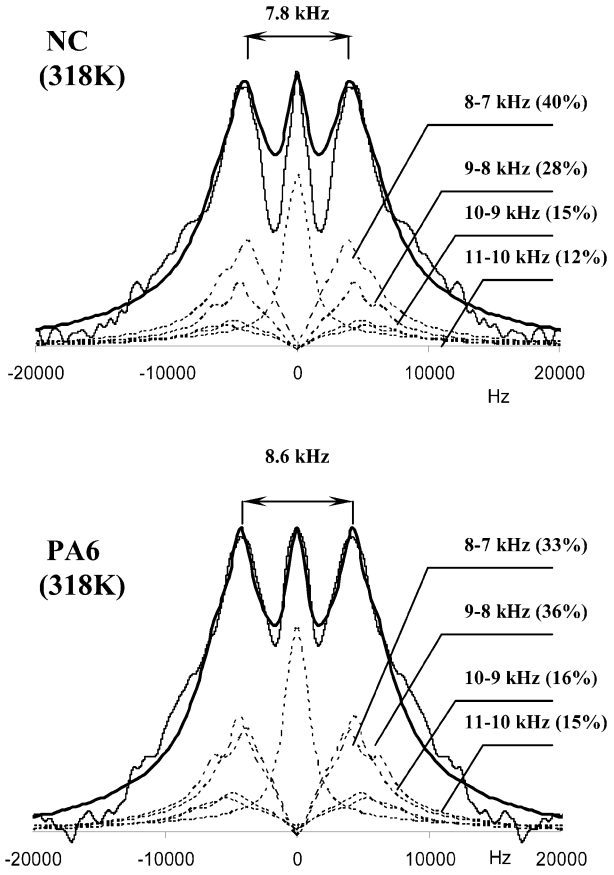

Figure 10. Decomposition of the $^{13}C-\{^1H\}$ dipolar spectra of methylene units C5 of neat polyamide-6 (PA6) and its nanocomposite (NC). Four dipolar doublets for the CH_2 spin system with scaled dipolar coupling constants in a fixed frequency range (11.0−10.0 kHz), (10.0−9.0 kHz), (9.0−8.0 kHz), and (8.0−7.0 kHz) were always used for the decomposition. The lines were broadened by a line-broadening factor of 1 kHz. Calculation of the line shapes was performed using time-independent zero-order Hamiltonian operating in zero-quantum spin space. The whole procedure was described previously.[43] The central signal was simulated by the Gauss−Lorentz function with a line width at half height of 4 kHz.

units of a highly mobile EMA elastomer. Consequently, the dipolar spectra are narrowed and the observed dipolar splitting is reduced.

To investigate internal dynamics of polymer segments in an amorphous phase close to T_g, the same 2D solid-state NMR experiments were repeated at a high temperature of 318 K (Figure 8). In both cases (at 308 and 318 K), the same tendencies were observed.

Discussion

Quality of the Dipolar Spectra. It has long been recognized that polymer chain dynamics exhibiting varying amplitudes and geometries such as small-amplitude librations, aromatic ring flips, discrete jumps of aliphatic side chains, and methyl rotations significantly affects the mechanical properties of synthetic polymers. That is why the investigation of the dynamics of polymer nanocomposites represents one of the forefronts of material science.

It is not surprising, however, that a detailed description of internal dynamics of complex polymer nanocomposites that are usually motionally heterogeneous and semicrystalline requires application of specific procedures. Generally, because of the limited spectral resolution, standard experimental techniques very often provide data averaged over several structure units and in some cases even over the whole sample. In the particular case of nanocomposites based on polyamides, the obtained dipolar data represent a superposition of the contributions of several polymorphic forms (Figure 9a) where the interference of the overlapping NMR signals leads to the debasement of the experimental results. Notice that, although the crystallinity of the studied systems is relatively low (ca. 30%), the resulting dipolar profiles are dominated by dipolar couplings typical for the crystalline phase. The detected splitting between the maxima is, however, slightly reduced (at about 1 kHz) due to the destructive interference with the dipolar signal of the amorphous component. That is why the application of selective techniques is necessary. Owing to this approach, the dipolar profiles corresponding to the amorphous phase and crystallites are clearly separated (Figure 9b and c).

Several repeated independent measurements confirmed that dipolar coupling constants are measured with an accuracy of ca. ±0.2 kHz. To exclude the effect of frequency offset on the quality of the dipolar spectra, we performed additional experiments with the ^{13}C carrier frequency shifted about ca. 60 ppm. No significant changes in the splitting of the dipolar spectra were observed, and the resolved differences were in the limit of the experimental error (±0.2 kHz, Supporting Information). And finally, to reduce the influence of electronic noise on the accuracy of measurements of dipolar splitting, all the dipolar spectra were decomposed by the peak fitting, as shown in Figure 10. The dipolar splitting was then determined from the envelope line. Consequently, we suppose that the differences in the splitting of dipolar spectra larger than 0.4 kHz can be interpreted as a change in the segmental dynamics of polymer segments without any doubt. In some cases, around the central peak, we observed large discrepancies between the spectra and the best fits (top Figure 10). This follows from the complex origin of the central part of the dipolar spectra resulting from a mixture of several contributions, as discussed later.

Influence of Paramagnetic Fe^{3+} Ions. In this connection, we have to analyze the possible influence of Fe^{3+} ions located in octahedral sites of silicate platelets. Fluctuating local dipolar fields of the unpaired electrons of Fe^{3+} ions completely destroy the coherence of ^{13}C and ^{1}H spins as close as 0.4 nm from the clay surface.[24,39] Consequently, at proper recoupling conditions, the ^{13}C magnetization predominantly evolves under the influence of dipolar coupling with ^{1}H spins, while the coupling with dipolar fields of the unpaired electrons is limited to a small fraction of polymer chains. The former contribution produces dipolar oscillation of ^{13}C magnetization detected during the recoupling period (t_1, Scheme 1), for which the frequency is reflected by the splitting in dipolar spectra. The frequency of this oscillation is, however, fairly insensitive to the presence of paramagnetic ions. The residual coupling with dipolar fields of Fe^{3+} rather induces the accelerated loss of spin coherence and thus the rapid decay of ^{1}H and ^{13}C magnetization. As proton spin diffusion that could propagate this behavior to a remote part of the polymer matrix is quenched by Lee−Goldburg irradiation, the rapid relaxation is localized only to a relatively small fraction of polymer chains. Nevertheless, this process still causes homogeneous broadening of the NMR signals, which in principle can influence the splitting of the asymmetric dipolar lines (Figure 5). However, as followed from our simulations, the splitting of the dipolar doublet remains approximately constant even when applying huge line broadening (LB = 5 kHz, CH_2 of glycine, Supporting Information). The observed changes in the splitting are ca. ±0.2 kHz. This is still in the range of the expected experimental error, and from this follows that the presence of Fe^{3+} ions in polymer systems cannot substantially change the detected value of dipolar coupling constants D_{CH}. Therefore, the applied PISEMA-type experiments can be interpreted in terms of motional amplitudes of polymer segments even in polymer systems containing paramagnetic ions. Such information then can be related to the mechanical properties of complex semicrystalline nanocomposites.

Segmental Dynamics in Crystallites. Measurement of one-bond $^{13}C-^{1}H$ dipolar couplings and determination of the order parameter is the simplest way to obtain information about segmental dynamics. In general, the order parameter, S, is a measure of the equilibrium distribution of orientations of the bond vector $\mu(t)$ in a molecular reference frame and ranges from 1 for fixed vectors to 0 for freely moving vectors. In the simplest case, assuming segmental motion to be axially symmetric and small in amplitude ($\langle \sin\theta \rangle \approx \langle\theta\rangle$), the order parameter can be converted to a root mean square (rms) angular fluctuation of the bond vector, $\sqrt{\langle\theta^2\rangle}$, according to the following definition[42,44]:

$$S = 1 - \frac{3}{2}\langle\theta^2\rangle \qquad (1)$$

As the motional amplitudes in crystalline domains of polyamide-66 measured at room temperature[45] are expected to be about 10°, this simplest but still physically realistic model of small-amplitude librations can be applied. For the order parameters reaching the values $S = 0.95-0.85$, the systematic error following from the Taylor expansion is almost negligible. The difference between $\sin\theta$ and θ is only ~2°, indicating that this analysis is adequate to describe motional behavior in crystallites of PA6. The acceptable difference[44] between $\sin\theta$ and θ is approximately 4°, which limits the application of this model for the order parameters larger than ca. $S = 0.6$.

In contrast to crystallites of small organic molecules where internal dynamics are almost quenched, the determined amplitudes of reorientation of CH_2 units of PA6 reach about 10−17° and increase from NH and CO groups to the central part of the repeat unit (Figure 6). This finding is in good accord with the data[45] previously reported for polyamide-66. In addition, from the direct comparison of the dipolar profiles produced by C1 methylene groups (Figure 11a), it is clear that segments in γ-form exhibit significantly enhanced motional amplitudes.

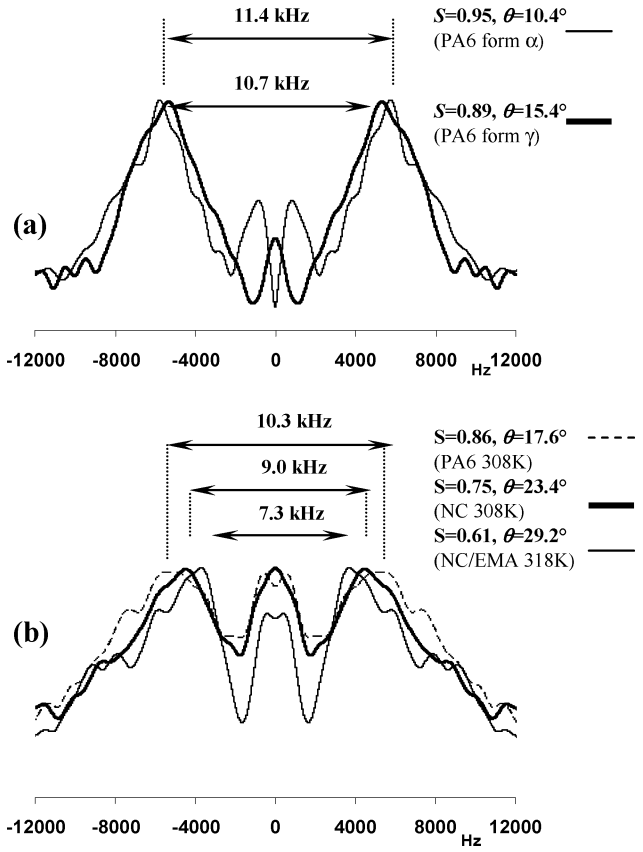

Figure 11. Superposition of the $^{13}C-\{^{1}H\}$ dipolar spectra of methylene units C1 of polyamide-6 chains in crystal α-form and γ-form (a). Superposition of $^{13}C-\{^{1}H\}$ dipolar spectra of methylene units C1 of polyamide-6 chains in the amorphous phase of pure polyamide-6 and its nanocomposites NC and NC/EMA (b).

The observed enhancement (ca. 5°) probably results from the altered conformation and packing of polymer chains in γ-crystallites.[46,47] As suggested by Lincoln et al.,[48] the addition of clay layers forces the amide groups of PA6 out of the plane formed by polymer chains. Resulting conformation changes then complicate formation of H-bond sheets. Consequently, in the melt, partially ordered polymer chains close to the clay surface are suitably oriented to crystallize in the thermodynamically unstable but kinetically favored γ-form. This crystallization does not require long crystallization time and large space, which is necessary for the folding of polymer chains into antiparallel orientation in the α-form. The resulting parallel orientation of the macromolecules in γ-form rather adopts twisted conformation, which is stabilized by intermolecular hydrogen bonds similarly as in the amorphous phase. This is why the resulting packing of macromolecules in the γ-form is less tight. Large free volume then permits not only higher frequency but also larger amplitudes of reorientation of polymer segments. Consequently, mechanical stress can be efficiently absorbed, and thermally activated chain translation through the γ-crystallites is allowed. This can lead to the larger deformability of the γ-form as recently observed.[49]

Motional Amplitudes in the Amorphous Phase. In contrast to crystallites, the segmental motion in the amorphous phase is

rather complex. This follows from the fact that, in semicrystalline and/or nanocomposite systems, it is reasonable to expect the existence of two subpopulations within the amorphous domains. Then a bimodal model[45] is the simplest model consistent with the experimental data. It is supposed that relatively restricted librational motion dominates in "constrained" domains, while fast trans−gauche two-site tetrahedral jumps operate in the "free" domains.[50] Both of these motional modes are probably reflected by the recorded dipolar spectra (Figure 7). While low-amplitude librations are reflected by the outer doublets, central signals with frequencies close to zero can correspond to high-amplitude jumps. Similarly, as in the previous case, the order parameters determined from the splitting of the outer doublets were converted to amplitudes of the axially symmetric librations (eq 1). The resulting motional amplitudes (rms angles 18−33 ± 0.7°, Figures 7 and 8) are comparable with the data recently reported[50] for polymer segments in constrained domains of the amorphous phase of polyamide-66. In general, in the amorphous phase, more complicated motions can be expected, and other models providing a more instructive picture can be applied (e.g., diffusion motion on the cone[51] or Gaussian axial fluctuation model[52]). Utilization of these models, however, requires more assumption and adjustable parameters. The current analysis highlights the changes in segmental mobility without relying on specific motional models. On the other hand, the central signals reflecting rapid jumps of the bond vector between N distinct orientations have to be analyzed according to the following relation:[53]

$$S^2 = \sum_{i,j=1}^{N} p_i p_j P_2(\cos \theta_{ij}) \qquad (2)$$

in which p is the equilibrium population of vector having the ith orientation, and θ_{ij} is the angle between vectors having the ith and jth orientations. In this case, the order parameter was estimated after the deconvolution from the line with of the central signal (ca. 4.0 kHz, Figure 10). Expecting, e.g., two-site jumps with equal populations, the order parameter $S = 0.33$ was converted to the C−H vector reorientation angle θ_{ij} ca. 108−110°. This well corresponds to trans−gauche transition. But in this case we must admit that the central signals with frequencies close to zero can in principle originate from a mixture of several contributions. In addition to motionally averaged interactions, also weak long-range $^1H-^{13}C$ dipolar couplings, incompletely refocused homonuclear $^1H-^1H$ dipolar couplings, and the inhomogeneity of the B_1 field in the probe head may affect the central signal.[29,30] In addition, in the case of such high-amplitude jumps, the asymmetry parameter of dipolar tensor no longer remains zero. Consequently, the shape of the dipolar spectra is significantly affected.[31] That is why these signals must be interpreted very cautiously and their information content must be considered to be very limited.

Internal Dynamics in Nanocomposites. The last question that should be opened concerns the dynamics of the amorphous phase in nanocomposites and the directly related glass-transition temperature (T_g) and other mechanical properties. The glass transition is one of the most important thermomechanical material properties of glassy and semicrystalline polymers affecting the mechanical behavior of manufactured products. Consequently, T_g, which is closely connected with the segmental dynamics of polymer chains, in many cases dictates the applications of polymer materials.

Usually, it is supposed that the presence of solid filler, to which a polymer matrix is either chemically attached or strongly absorbed, leads to an increase in T_g as a result of sterically hindered segmental motions. However, in nanocomposites, this relation is not so simple, and the presence of layered silicates in polyamide-6 matrix causes a slight decrease in T_g (Figure 1). This phenomenon can be related to a recent observation indicating that silicate layers weaken hydrogen bonding not only in the γ-form but also in α-crystallites of the polyamide.[53] This is explained by steric hindrances, which do not allow suitable reorientation of amide groups for optimal formation of hydrogen bonding.[53] Then, the crystallization in thermodynamically less advantageous conformation is favored.

As clearly reflected by the reduced splitting of the dipolar spectra (Figure 11b), the dynamics of polymer segments C1 and C5 in the amorphous phase is notably enhanced in the presence of the silicate platelets. This indicates that, in the nanocomposites, the average motional amplitudes of polymer segments close to amide groups are increased probably due to the weakened intermolecular hydrogen bonds. This behavior can result from the same process, which reduces hydrogen-bond strength in the crystallites, as mentioned above.[53] Further, we can expect the presence of local fluctuations in the density of polymer chains in the amorphous phase induced by silicate nanoparticles. These silicate sheets with a diameter 75−150 nm across together with crystallites of PA6 can form a framework somewhat bracing the polymer matrix that does not allow contraction and tight packing of polymer chains in the amorphous phase after the crystallization. Consequently, the presence of clay nanoparticles leads to the formation of local density inhomogeneities. At the low-density regions, relatively far from the silicate surface and γ-crystallites, the strength of the intermolecular hydrogen bonds is reduced and the increased free volume allows enhancement of librational amplitudes of polymer segments.

An alternative explanation of the enhanced segmental dynamics in nanocomposites published by Yang et al.[54] operates with the fact that, in tightly confined environments, it may be difficult for macromolecules to adopt their lowest energy conformation. This may lead to the enhancement of low-amplitude reorientation due to inefficiencies in packing and lack of access to low energy conformations. However, these effects must be balanced by the interactions of other parts of polymer layer with the inorganic surface. From this follows the existence of broader distribution of internal dynamics in nanocomposites. This phenomenon has been recently observed for poly(ϵ-caprolactone)[55] and polystyrene[56] nanocomposites, and molecular dynamics computer simulations[56] suggest that the thickness of the layers exhibiting steep changes in segmental dynamics can be as few as 0.5 nm. In our particular case, the existence of both rigid and more mobile fractions in the amorphous phase was ascertained in all of the investigated polymer systems. In all cases, the corresponding dipolar spectra were decomposed to several contributions (Figure 10). This follows from the fact that even neat polyamide-6 can be considered as an nanocomposite because the size of crystallites that are embedded in an amorphous matrix is ca. 4−8 nanometers.[49]

An additional slight increase in motional amplitudes observed in the triple-component system NC/EMA can be attributed to the increase in concentration of silicate platelets in a PA6 matrix. Because of the total immiscibility of silicate particles in EMA copolymer (Figure 4), the amount of silicate sheets in the amorphous phase of PA6 is effectively increased, which probably increases the extent of local density fluctuation. The presence of EMA copolymer further affects the pattern of the dipolar profiles separated at ca. 30 ppm (Figures 8 and 9). An

apparent narrowing of these spectra follows from the superposition and interference of dipolar contributions originating from methylene groups, C2, and ethylene units of EMA elastomer. This indicates that the size of phase-separated domains of EMA elastomer (50−200 nm) is large enough for the internal dynamics and was not affected by the glassy matrix of PA6 and clay particles. Consequently, high segmental dynamics of EMA copolymers is retained and almost unchanged.

From the thermodynamic point of view, the determination of the order parameters in the repeat unit makes it possible to quantitatively express the increase in motional amplitudes in nanocomposites as a change in the Gibbs free energy resulting from the increase in conformational entropy:[57]

$$\Delta G = -kT \sum_n \ln\left(\frac{1 - {S_{n2}}^2}{1 - {S_{n1}}^2}\right) \tag{3}$$

The term, ${S_{nk}}^2$, is the order parameter for the nth spin in the kth state and the summation extends over all affected nuclei. In both types of the nanocomposites, the Gibbs free energy is slightly reduced ($\Delta G = 0.4-0.5$ kcal/mol), and although this entropic contribution is not very large in the continuous amorphous phase, this change may be correlated with the observed decrease in T_g.

To better understand motional behavior of the nanocomposites, we tried to probe segmental dynamics of polymer chains in the amorphous phase close to T_g. However, the crystal γ modification is thermodynamically unstable, and at such a high temperature (ca. 55−60 °C), a transition into the stable α-form can occur. To avoid this problem, we increased the experimental temperature to only 45 °C at which no changes in composition of polymer systems were observed. In all investigated polymer systems, the elevated temperature causes the decrease in the order parameter, S, which indicates enhanced librational amplitudes of polymer segments. At the same time, the differences in the motional amplitudes between polymer chains in the amorphous phase of neat polyamide-6 and its nanocomposites persist, confirming that the small-angle librations of polymer segments are thermally activated. From this follows that the fast segmental flips in the nanosecond time scale with relatively low amplitudes around 15−30° occurring in a glassy state can be considered as mechanically active and as a potential factor that may help to enable the larger-amplitude motions (jumps) associated with glass-transition temperature. The most prominent temperature-induced changes in the overall shape of the dipolar spectra observed for ethylene units of EMA copolymer then confirm that, in the phase-separated domains, relatively high-amplitude thermally activated motions occur. If these motions are attributed to the chain translations through the domains, then they will contribute to the enhancement of toughness and elongation at brake of the triple-component system. These contributions then act simultaneously with the changes in morphology (formation of core−shell particles of elastomer) and lead to a significant improvement in mechanical properties.

Conclusion

In this contribution, two different recoupling solid-state NMR techniques were employed to probe the mobility of polymer chains separately in amorphous and crystalline phases of semicrystalline nanocomposites based on polyamide-6 and layered silicates. Segmental dynamics of polymer chains in pure polyamide-6, a simple double-component system, and toughness-enhanced triple-component nanocomposites, was investigated. Motional amplitudes were successfully determined for all resolved methylene units in the crystallites in the "constrained" domains as well as in the "free" domains of the amorphous phase of polyamide-6. We demonstrated that the applied experimental procedures provided high-quality data, for which accuracy was sufficiently high to clarify the observed changes in thermomechanical properties of the polymer systems. Particular attention was devoted to the discussion of the observed decrease in T_g in both double- and triple-component nanocomposites and to the significant increase in toughness observed in the triple-component system containing phase-separated domains of elastomer. In all cases, we tried to correlate these changes with the enhanced motional amplitudes of polymer chains in the amorphous phase.

Acknowledgment. We thank the Grant Agency of the Czech Republic (grant 106/03/0679) the Grant Agency of the Academy of Sciences of the Czech Republic (grant IAA400500602), and Ministry of Education, Youth and Sports, (grant 2503/2005) for financial support.

Supporting Information Available: Figures of optimization of the recoupling sequence, static ^{1}H NMR spectra, broadening of dipolar doublets as well as dipolar spectra measured at various offset. This material is available free of charge via the Internet at http://pubs.acs.org.

References and Notes

(1) *Polymer−Clay Nanocomposites*; Pinnavaia T. J., Beall G. W., Eds.; John Wiley & Sons: New York, 2001.
(2) Liu, L.; Qi, Z.; Zhu, X. *J. Appl. Polym. Sci.* **1999**, *71*, 1133.
(3) Xiong, M.; Gu, G.; You, B.; Wu, L. *J. Appl. Polym. Sci.* **2003**, *90*, 1923.
(4) Sun, Y.; Zhang, Z.; Moon, K.-S.; Wong, C. P. *J. Polym. Sci., Part B: Polym. Phys.* **2004**, *42*, 3849.
(5) Ash, B. J.; Schadler, L. S.; Siegel, R. W. *Mater. Lett.* **2002**, *55*, 83.
(6) Kalgaonkar, R. A.; Jog, J. P. *J. Polym. Sci., Part B: Polym. Phys.* **2001**, *41*, 3102.
(7) Wu, Z.; Zhou, Ch.; Qi, R.; Zhang, H. *J. Appl. Polym. Sci.* **2002**, *83*, 2403.
(8) Park, J.; Jana, S. C. *Macromolecules* **2003**, *36*, 8391.
(9) Han, B.; Cheng, A.; Ji, G.; Wu, S.; Shen, J. *J. Appl. Polym. Sci.* **2004**, *91*, 2536.
(10) Tjong, S. C.; Bao, S. P. *J. Polym. Sci., Part B: Polym. Phys.* **2004**, *42*, 2878.
(11) Liu, Z.; Chen, K.; Yan, D. *Eur. Polym. J.* **2003**, *39*, 2359.
(12) Shelley, J. S.; Mather, P. T.; De Vries, K. L. *Polymer* **2001**, *42*, 5849.
(13) Pramoda, K. P.; Liu, T. *J. Polym. Sci., Part B: Polym. Phys.* **2004**, *42*, 1823.
(14) Lincoln, D. M.; Vaia, R. A.; Wang, Z.-G.; Hsiao, B. S.; Krishnamoorti, R. *Polymer* **2001**, *42*, 9975.
(15) Hou, S. S.; Bonagamba, T. J.; Beyer, F. L.; Madison, P. H.; Schmidt-Rohr, K. *Macromolecules* **2003**, *36*, 2769.
(16) Ying, D. K.; Zax, D. B. *J. Phys. Chem.* **1999**, *110*, 5325.
(17) Hou, S. S.; Beyer, F. L.; Schmidt-Rohr, K. *Solid State Nucl. Magn. Reson.* **2002**, *22*, 110.
(18) De Paul, S. M.; Zwanziger, J. W.; Ulrich, R.; Wiesner, U.; Spiess, H. W. *J. Am. Chem. Soc.* **1999**, *121*, 5736.
(19) Pawsey, S.; McCormick, M.; De Paul, S.; Graf, R.; Lee, Y. S.; Reven, L.; Spiess, H. W. *J. Am. Chem. Soc.* **2003**, *125*, 4174.
(20) Brus, J.; Dybal, J.; Schmidt, P.; Kratochvíl, P.; Baldrian, J. *Macromolecules* **2000**, 33, 6448.
(21) Brus, J.; Spirkova, M.; Hlavata, D.; Strachota, A. *Macromolecules* **2004**, *37*, 1346.
(22) Brus, J.; Dybal, J, *Macromolecules* **2002**, *35*, 10038.
(23) Brus, J.; Dybal, J.; Sysel, P.; Hobzová, R. *Macromolecules* **2002**, *35*, 1253.
(24) Van der Hart, D. L.; Asano, A.; Gilman, J. W. *Macromolecules.* **2001**, *34*, 3819.
(25) Spiess, H. W. *Colloid Polym. Sci.* **1983**, *261*, 193.
(26) Fisbach, I.; Ebert, F.; Spiess, H. W.; Schnell, I. *Chem. Phys. Chem.* **2004**, *5*, 895.
(27) Saalwächter, K.; Schnell, I. *Solid State Nucl. Magn. Reson.* **2002**, *22*, 154.
(28) Lee, M.; Goldburg, W. *Phys. Rev.* **1965**, *140*, A1261.

(29) van Rossum, B. J.; de Groot, C. P.; Ladizhansky, V.; Vega, S.; de Groot, H. J. M. J. *Am. Chem. Soc.* **2000**, *122*, 3465.
(30) Ladizhansky, V.; Vega, S. *J. Chem. Phys.* **2000**, *112*, 7158.
(31) Hong, M.; Yao, X.; Jakes, K.; Huster, D. *J. Phys. Chem. B* **2002**, *106*, 7355.
(32) Dvinskikh, S. V.; Zimmermann, H.; Maliniak, A.; Sandstrom, D. *J. Magn. Reson.* **2003**, *164*, 165.
(33) Wu, C. H.; Ramamoorthy, A.; Opella, S. J. *J. Magn. Reson., Ser. A* **1994**, *109*, 270.
(34) Brus, J.; Urbanova, M. *J. Phys. Chem. A* **2005**, *109*, 5050.
(35) Torchia, D. A. *J. Magn. Reson.* **1978**, *30*, 613.
(36) Bennett, A. E.; Rienstra, C. M.; Auger, M.; Lakshmi, K. V.; Griffin, R. G. *J. Chem. Phys.* **1995**, *103*, 6951.
(37) Brus, J. *Solid State Nucl. Magn. Reson.* **2000**, *16*, 151.
(38) Hatfield, G. R.; Glans, J. H.; Hammond, W. B. *Macromolecules* **1990**, *23*, 1654.
(39) Van der Hart, D. L.; Asano, A.; Gilman, J. W. *Chem. Mater.* **2001**, *13*, 3796.
(40) Kelnar, I.; Kotek, J.; Kaprálková, L.; Munteanu, B. S. *J. Appl. Polym. Sci.* **2005**, *96*, 288.
(41) Kelnar, I.; Kotek, J.; Kaprálková, L.; Hromádková, J.; Kratochvíl, J. *J. Appl. Polym. Sci.* **2006**, *100*, 1571.
(42) Palmer, A. G.; Williams, J.; McDermott, A. *J. Phys. Chem.* **1996**, *100*, 13293.
(43) Brus, J.; Jakeš, J. *Solid State Nucl. Magn. Reson.* **2005**, *27*, 180.
(44) Huster, D.; Xiao, L.; Hong, M. *Biochemistry* **2001**, *40*, 7662.
(45) Hirschinger, J.; Miura, H.; Gardner, K. H.; English A. D. *Macromolecules.* **1990**, *23*, 2153.
(46) Schreiber, R.; Veeman, W. S.; Gabriëlse, W.; Arnauts, J. *Macromolecules* **1999**, *32*, 4647.
(47) Li, Y.; Goddard, W. A., III. *Macromolecules* **2002**, *35*, 8440.
(48) Lincoln, D. M.; Vaia, R. A.; Wang, Z. G.; Hsiao, B. S. *Polymer* **2001**, 42, 1621.
(49) Konishi, R.; Ito, M. *Polymer* **2004**, *45*, 5191.
(50) Miura, H.; Hirschinger, J.; English A. D. *Macromolecules* **1990**, *23*, 2169.
(51) Lipari, G.; Szabo, A. *J. Am. Chem. Soc.* **1982**, *104*, 4546.
(52) Brüschweiler, R.; Wright, P. E. *J. Am. Chem. Soc.* **1994**, *116*, 8426.
(53) Wu, Q.; Liu, X.; Berglund L. A. *Polymer* **2002**, *43*, 2445.
(54) Yang, D.-K.; Zax, D. B. *Solid State Nucl. Magn. Reson.* **2006**, *29*, 153.
(55) Hrobarikova, J.; Robert, J. L.; Calberg, C.; Jerome, R.; Grandjean, J. *Langmuir* **2004**, *20*, 9829.
(56) Zax, D. B.; Yang, D.-K.; Santos, R. A.; Hegemann, H.; Giannelis, E. P.; Manias, E *J. Chem. Phys* **2000**, *112*, 2945.
(57) Akke, M.; Brüschweiler, R.; Palmer, A. G. *J. Am. Chem. Soc.* **1993**, *115*, 9832.

MA0604946